Available online at www.sciencedirect.com
ScienceDirect
Journal of Physics and Chemistry of Solids 69 (2008) 1623–1631
JOURNAL OF PHYSICS AND CHEMISTRY OF SOLIDS
www.elsevier.com/locate/jpcs

Photoactive materials prepared by homogeneous hydrolysis with thioacetamide: Part 2—TiO_2/ZnO nanocomposites

Vendula Houšková[a,b,*], Václav Štengl[a], Snejana Bakardjieva[a], Nataliya Murafa[a]

[a]*Institute of Inorganic Chemistry, Academic of Sciences of the Czech Republic, Rez 250 68, Czech Republic*
[b]*Institute of Polymeric Materials, Faculty of Chemical Technology, University of Pardubice, nám. Cs. Legií 562, Pardubice 532 10, Czech Republic*

Received 3 August 2007; received in revised form 21 November 2007; accepted 30 November 2007

Abstract

Photocatalytic active titanium dioxide (TiO_2)/zinc oxide (ZnO) composite was prepared by homogeneous hydrolysis of a mixture of titanium oxo-sulphate and zinc sulphate in aqueous solutions with thioacetamide and subsequent annealing at the temperature of 600 °C. The prepared samples were characterized by X-ray diffraction (XRD), scanning electron microscopy (SEM) and high-resolution transmission microscopy (HRTEM). Nitrogen adsorption–desorption was used for surface area (Brunauer–Emmett–Teller—BET) and porosity determination. The photoactivity of the prepared TiO_2/ZnO samples was assessed by the photocatalytic decomposition of Orange II dye in an aqueous slurry under irradiation of 254 and 365 nm wavelengths. Under the same conditions, the photocatalytic activity of a commercially available photocatalyst (Degussa P25), the pure anatase TiO_2 nanoparticles and cubic ZnO were examined.

1. Introduction

Photocatalytic degradation processes have been widely applied as techniques of destruction of organic pollutants in wastewater and effluents. Titanium dioxide (TiO_2) has been extensively investigated as one of the most active semiconductor photocatalysts [1]. It has been known that zinc oxide (ZnO) is a suitable alternative to TiO_2 so far as band-gap energy is concerned, and in fact higher photocatalytic efficiency compared with TiO_2 has been reported for ZnO [2–4].

TiO_2 is widely used for photocatalytic air and water purification and many other purposes based on photocatalytic oxidation and decomposition of organic pollutants [5–7]. This material can also be used for solar energy storage and conversion [8], organic syntheses [9], etc. TiO_2 is one of the most popular and promising materials for these purposes, because of its stability, commercial availability and ecological safety. According to the literature [10–12], the photocatalytic activity of suspended TiO_2 in solution strongly depends on the physical properties of TiO_2 (e.g. crystallinity, crystal structure, surface area, surface hydroxyls and particle size).

In order to enhance the activity of the catalyst, many efforts have been made to modify TiO_2 by adding ZnO as a photocatalyst [13–15]. Various preparation methods of ZnO nanoparticles [16–20] and their size-dependent electronic [21] and optical [22] properties have been studied extensively for specific applications such as catalysts, photovoltaic and electroluminescent devices and functional devices (sensor, varistor, etc). In general, the physical, chemical and photochemical properties of the ZnO nanoparticles are different depending on the manufacturing method [23–27].

In this contribution, a binary oxide catalyst TiO_2/ZnO was prepared by homogeneous hydrolysis of zinc sulphate, titanium oxo-sulphate ($TiOSO_4$) and thioacetamide (TAA) at 80 °C and later controlled annealing in oxygen atmosphere at the temperature of 600 °C. The photocatalytic activity of the TiO_2/ZnO composite was tested by degradation of an aqueous solution of 0.02 M Orange II (OII) dye at wavelengths of 254 and 365 nm. Under the same

*Corresponding author at: Institute of Polymeric Materials, Faculty of Chemical Technology, University of Pardubice, nám. Cs. Legií 562, Pardubice 532 10, Czech Republic. Tel.: +420 2 6617 3534; fax: +420 2 2094 0257.
E-mail address: houskova@iic.cas.cz (V. Houšková).

0022-3697/$ - see front matter © 2008 Elsevier Ltd. All rights reserved.
doi:10.1016/j.jpcs.2007.11.029

conditions, the photocatalytic activity of a commercially available photocatalyst (Degussa P25), the pure anatase TiO_2 and ZnO [4] nanoparticles were examined.

2. Experimental

2.1. Synthesis of TiO_2/ZnO nanocomposites

All used chemicals; $TiOSO_4$, zinc sulphate and TAA, were of analytical grade and were supplied by Fluka. $TiOSO_4$ and $ZnSO_4 \cdot 7H_2O$ (see Table 1) were dissolved in 4 L of distilled water and 100 g of TAA was added. The reaction mixture was adjusted to pH = 2 with sulphuric acid. The reaction mixture was heated at the temperature of 80 °C under stirring for 4 h. Thus-synthesized TiO_2/ZnS samples were washed with distilled water with decantation, filtered off, and dried at 105 °C in a drying kiln. After atmosphere annealing at the temperature of 600 °C in oxygen atmosphere for 1 h, samples of TiO_2/ZnO nanocomposites were observed. By this method, 12 TiO_2/ZnO specimens, denoted as TZO_0-TZO_11, were prepared.

2.2. Characterization methods

Surface areas of the samples were determined from nitrogen adsorption–desorption isotherms at liquid nitrogen temperature using a Quantachrom Nova2000 instrument with outgas for 15 min at 150 °C. The Brunauer–Emmett–Teller (BET) method was used for surface area calculation [28]; the pore size distribution (pore diameter and pore volume of the samples) was determined by the Barrett–Joyner–Halenda (BJH) method [29].

Transmission electron microscopy (TEM) and high-resolution transmission electron microscopy (HRTEM) micrographs were obtained by using two instruments, namely, Philips EM 201 at 80 kV and JEOL JEM 3010 at 300 kV (LaB_6 cathode). Copper grid coated with a holey carbon support film was used to prepare samples for the TEM observation. A powdered sample was dispersed in ethanol and the suspension was treated in an ultrasonic bath for 10 min.

Scanning electron microscopy (SEM) studies were performed using a Philips XL30 CP microscope equipped with energy-dispersive X-ray (EDX), Robinson, secondary electron (SE) and back-scattered electron (BSE) detectors. The sample was placed on an adhesive C slice and coated with a 10 nm thick layer of Au–Pd alloy.

X-ray diffraction (XRD) patterns were obtained by Siemens D5005 instrument using Cu Kα radiation (40 kV, 30 mA) and diffracted beam monochromator. Qualitative analysis was performed with the Eva Application and the Xpert HighScore using the JCPDS PDF-2 database [30]. The crystallite sizes of the samples were calculated from the Scherrer equation [31] using the XRD peak at $2\Theta = 25.2^\circ$ (anatase), $2\Theta = 27.4^\circ$ (rutile), $2\Theta = 36.2^\circ$ (zincite) and $2\Theta = 35.1^\circ$ (Zn_2TiO_4).

Photocatalytic activity of samples was assessed from the kinetics of the photocatalytic degradation of OII dye in aqueous slurries. The kinetics of photocatalytic degradation of aqueous OII dye solution was measured by using a self-constructed photoreactor [32,33]. The photoreactor consists of a stainless-steel cover and quartz tube with florescent lamp (254 and 365 nm) with power 8 W. OII dye solution was circulated by means of a membrane pump through flow cuvette. The concentration of OII dye was determined by measuring the absorbance at 480 nm with the VIS spectrofotometer ColorQuestXE.

3. Results and discussion

3.1. X-ray diffraction (XRD)

The powder XRD patterns of the TiO_2/ZnO composites prepared by homogeneous hydrolysis and subsequent annealing at 600 °C are shown in Figs. 1 and 2. From the XRD patterns and the corresponding characteristic 2Θ values of the diffraction peaks, it can be confirmed that the TiO_2 in as-prepared samples was identified as anatase

Table 1
Characteristics of prepared samples denoted as TZO_0–TZO_11

Sample	$TiOSO_4$ (g)	$ZnSO_4$ (g)	EDX of Ti (wt%)	EDX of Zn (wt%)	EDX of S (wt%)	BET ($m^2 g^{-1}$)	Pore radius (nm)	Pore volume ($cm^3 g^{-1}$)
TZO_0	0	100	–	82.09	0.86	5.6	0.17	0.018
TZO_1	4	96	3.53	78.92	0.11	6.9	0.17	0.011
TZO_2	9	91	7.70	70.25	0.21	12.5	0.15	0.018
TZO_3	18	82	30.71	30.85	0.76	2.9	0.17	0.005
TZO_4	36	64	32.18	26.45	0.65	10.4	0.17	0.018
TZO_5	50	50	34.25	21.19	0.82	28.2	0.17	0.041
TZO_6	75	25	44.43	1.44	0.71	37.4	0.17	0.041
TZO_7	85	15	54.97	1.55	1.11	61.7	0.17	0.065
TZO_8	90	10	54.35	0.26	0.77	66.9	0.19	0.093
TZO_9	95	5	50.12	0.12	0.54	72.5	0.24	0.105
TZO_10	97	3	48.90	0.5	0.71	79.6	0.25	0.115
TZO_11	100	0	56.23	–	0.30	108.8	0.17	0.121

Experimental conditions, energy dispersive X-ray analysis (EDX), BET surface areas and porosities of prepared samples.

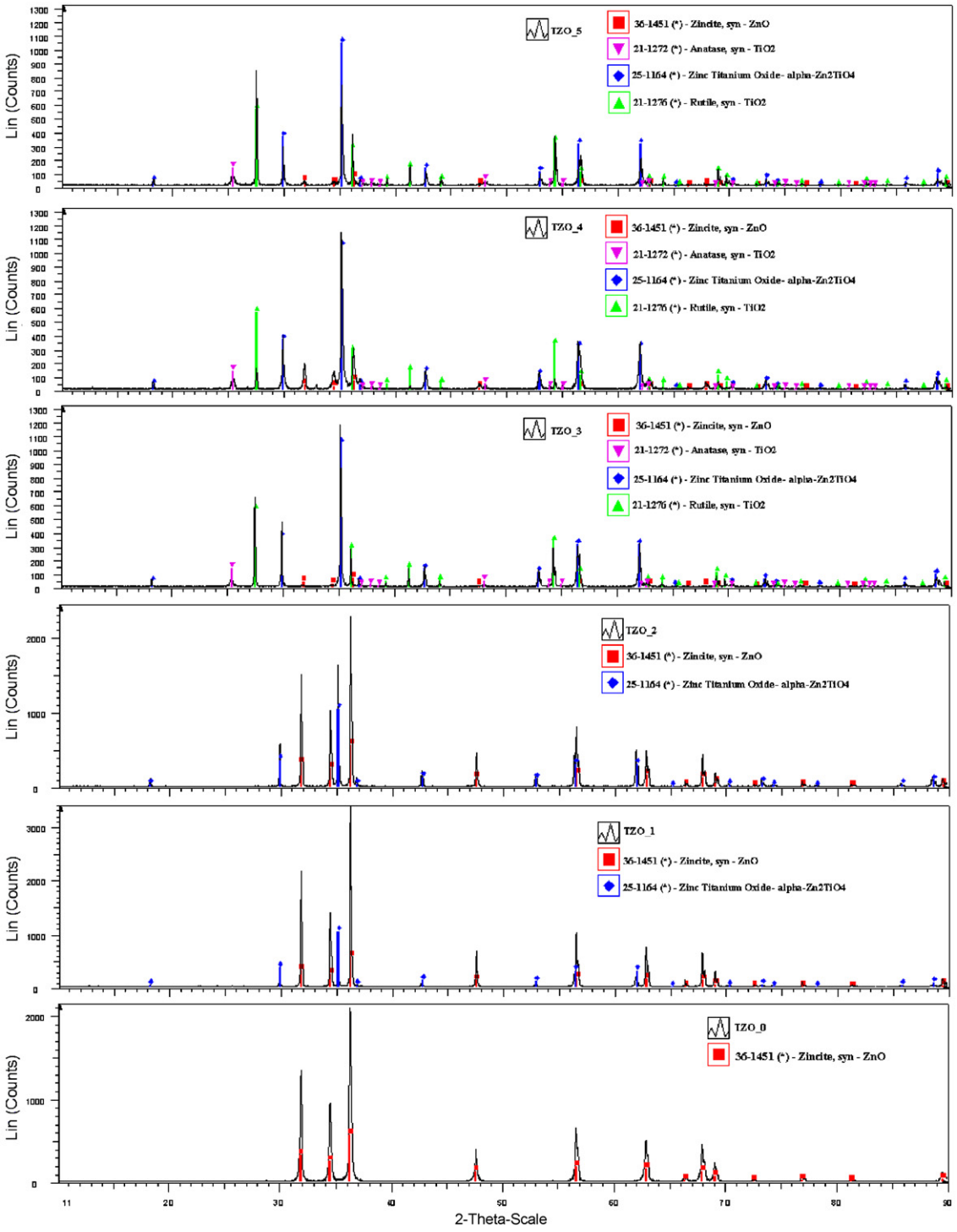

Fig. 1. XRD patterns of TiO_2/ZnO composite (samples TZO_0–TZO_5).

phase (JC PDF 21-1272) or rutile phase (JC PDF 21-1276), while the ZnO was zincite phase (JC PDF 36-1451). In addition, zinc titanium oxide phase (JC PDF 25-1164) was identified in some specimens. In samples TZO_1 and TZO_2, which were poorer in the starting compound $TiOSO_4$, only two phases—zincite and zinc titanium oxide, occurred. Samples denoted as TZO_3, TZO_4 and TZO_5 contain all four phases—anatase, rutile, zincite and zinc titanium oxide phase. In the case of samples TZO_6, TZO_7, TZO_8, TZO_9 and TZO_10, lower content of ZnO forms with anatase some kind of intra-particle structure. Samples TZO_0 and TZO_11 are pure forms of anatase and zincite.

The average size t of crystallites was calculated from the peak half-width B, using the Sherrer equation [31]

$$t = \frac{k\lambda}{B\cos\Theta}, \tag{1}$$

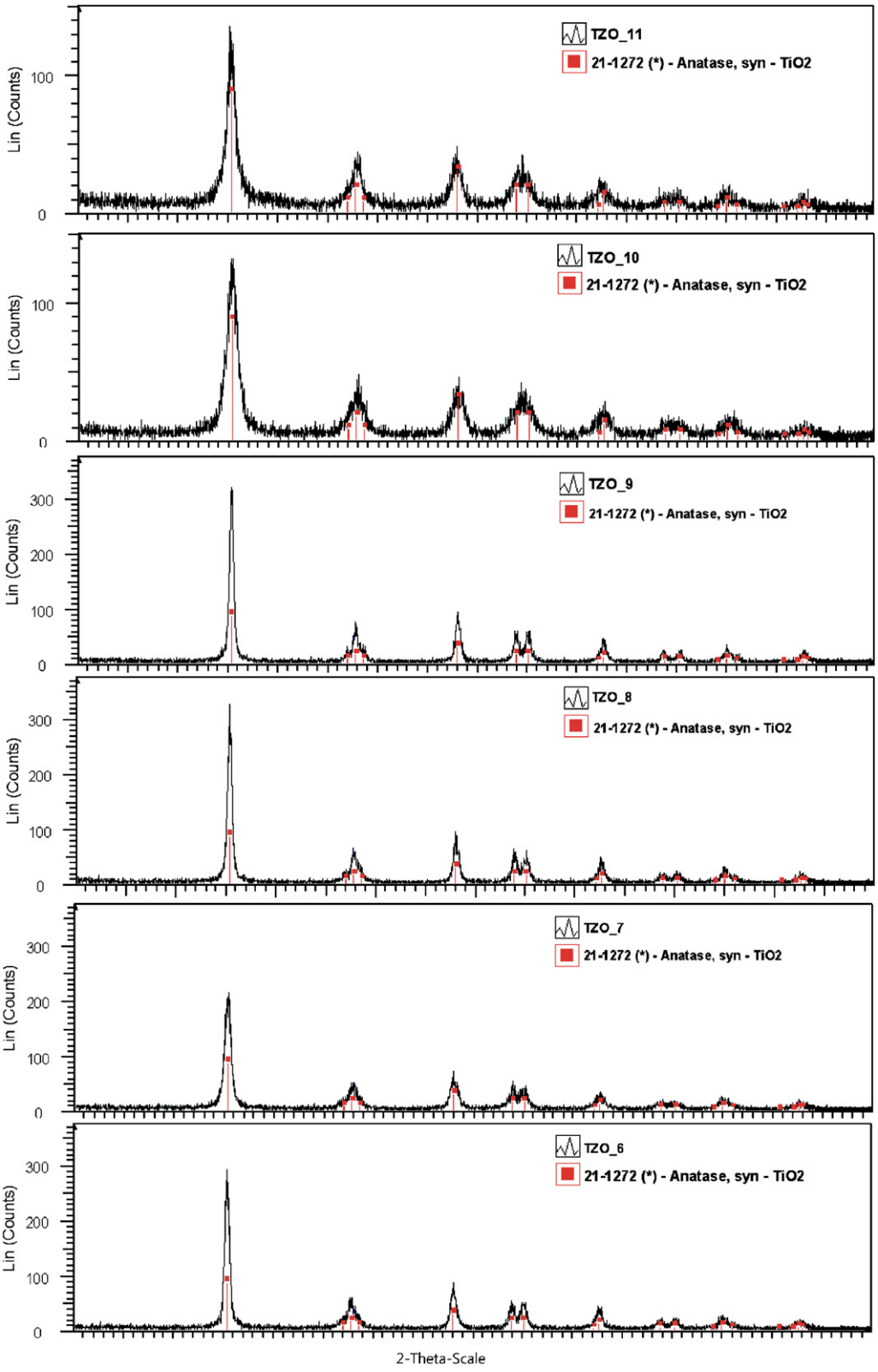

Fig. 2. XRD patterns of TiO_2/ZnO composite (samples TZO_6–TZO_11).

where k is a shape factor of the particle (it is 1 if the spherical shape is assumed) and λ and Θ are the wavelength and the incident angle of the X-rays, respectively. The peak width was measured at half of the maximum intensity. The crystallite sizes were calculated from diffraction plane (1 0 1) of anatase, diffraction plane

Table 2
Crystallite sizes of the anatase, rutile, zincite and zinc titanium oxide phases contained in prepared TiO_2/ZnO composites

Sample	Anatase crystallite size (nm)	Rutile crystallite size (nm)	Zincite crystallite size (nm)	Zn_2TiO_4 crystallite size (nm)
TZO_0	–	–	63.2	–
TZO_1	–	–	85.6	63.6
TZO_2	–	–	82.5	82.2
TZO_3	21.6	115.9	79.3	60.1
TZO_4	22.2	120.4	78.2	59.6
TZO_5	22.8	122.7	78.6	53.9
TZO_6	15.2	–	–	–
TZO_7	2.6	–	–	–
TZO_8	3.0	–	–	–
TZO_9	5.2	–	–	–
TZO_10	6.2	–	–	–
TZO_11	6.2	–	–	–

(1 1 1) of zincite, diffraction plane (1 1 0) of rutile and diffraction plane (1 0 0) of Zn_2TiO_4. The relative amount of anatase, rutile, zincite and Zn_2TiO_4, respectively, were calculated from the XRD patterns by PowderCell for Windows version 2.1 programme (see Table 2).

3.2. Surface area and porosity

BET Langmuir surface area of TiO_2/ZnO composite depend on the amount of TiO_2. The sample denoted as TZO_11 has the largest surface area ($108.8\,m^2\,g^{-1}$) (see Table 1). TiO_2/ZnO nanocomposites displayed a type-I isotherm with desorption hysteresis loop A [34]. Type a hysteresis is due principally to cylindrical pores open at both ends and the microporosity of pore size distribution is most often about pore diameter of 0.17 nm. Results from desorption BJH pore volume distribution and pore area distribution confirmed the microporous structure of prepared samples. The pore radius is in the interval 0.15–0.25 nm and the total pore volume is in the interval $0.005–0.12\,cm^3\,g^{-1}$ for TiO_2/ZnO nanocomposites.

3.3. Scanning electron microscopy (SEM)

The SEM micrographs of the prepared TiO_2/ZnO nanocomposites are presented in Fig. 3. It is obvious that the annealed product of homogeneous precipitation of TAA and zinc sulphate consists of approximate spherical round particle agglomerates of diameter about 2 μm (Figs. 3e, f), which are formed by spherical nanoparticles conjoined to the chains [4]. The annealed product of homogeneous hydrolysis of TAA and $TiOSO_4$ consists of approximate spherical agglomerates of diameter about 1 μm (Fig. 3(k)). The TiO_2/ZnO composites are formed with a mixture of single agglomerates of anatase, rutile, zincite or zinc titanium oxide. A special group is formed by overgrown agglomerates of TiO_2 and ZnO represented by TZO_6 to TZO_10 specimens.

3.4. High-resolution transmission electron microscopy (HRTEM)

Results obtained by HRTEM are shown in Fig. 4. The HRTEM micrographs in Figs. 4(a)–(d) characterized the surface morphology of the sample denoted as TZO_5. It is obvious that the nanoparticles of each phase form crystalline islands. The interlayer spacing is 0.352 nm, corresponding to the (1 0 1) plane of anatase (Fig. 4(d)), the interlayer spacing 0.324 nm, corresponding to the (1 1 0) plane of rutile (Fig. 4(b), phase no. 4), the interlayer spacing 0.247 nm, corresponding to the (1 0 1) plane of zincite (Fig. 4(c)) and the interlayer spacing 0.596 nm, corresponding to the (1 0 0) plane of Zn_2TiO_4 (Fig. 4(b), phase no. 3).

3.5. Photocatalytic activity

The photocatalytic activity of the prepared samples was determined by degradation of 0.02 M OII dye aqueous solutions at 254 and 365 nm radiation. In regions where Lamber–Beer law is validated, the concentration is proportional to absorbance:

$$A = \varepsilon c l, \tag{3}$$

where A is the absorbance, c the concentration of the absorbing component, l the length of the absorbing layer and ε the molar absorbing coefficient. The time dependences of OII dye decomposition can be described by using the following equation for the first kinetics reaction [35]:

$$\mathrm{d[OII]}/\mathrm{d}t = k(a_0 - \mathrm{[OII]}), \tag{4}$$

where [OII] is the concentration of OII dye, a_0 the initial concentration of OII dye and k the rate constant. For comparison, the photocatalytic activity of a commercially available photocatalyst Degussa P25, anatase TiO_2 or ZnO nanoparticles were tested. The calculated degradation rate constants are listed in Table 3 and examples of kinetic degradation of OII dye at 254 and 365 nm wavelength using samples TZO_0, TZO_7, TZO_10 and P25 are showed in Fig. 5. The highest degradation rate was achieved on the sample TZO_7 ($k = 0.1232$). This result corresponds to a high BET surface area ($61.7\,m^2\,g^{-1}$).

UV light provides the photons required for electron transfer from the valence band to conduction band of the photocatalyst. The energy of a photon is related to its wavelength and the overall energy input to a photocatalytic process is dependent on the light intensity. Therefore, the effect of both intensity and wavelength is important. Matthews and McEvoy [36] showed that shorter wavelength (254 nm) radiation is considerably more effective in promoting degradation than radiation centred at 350 nm

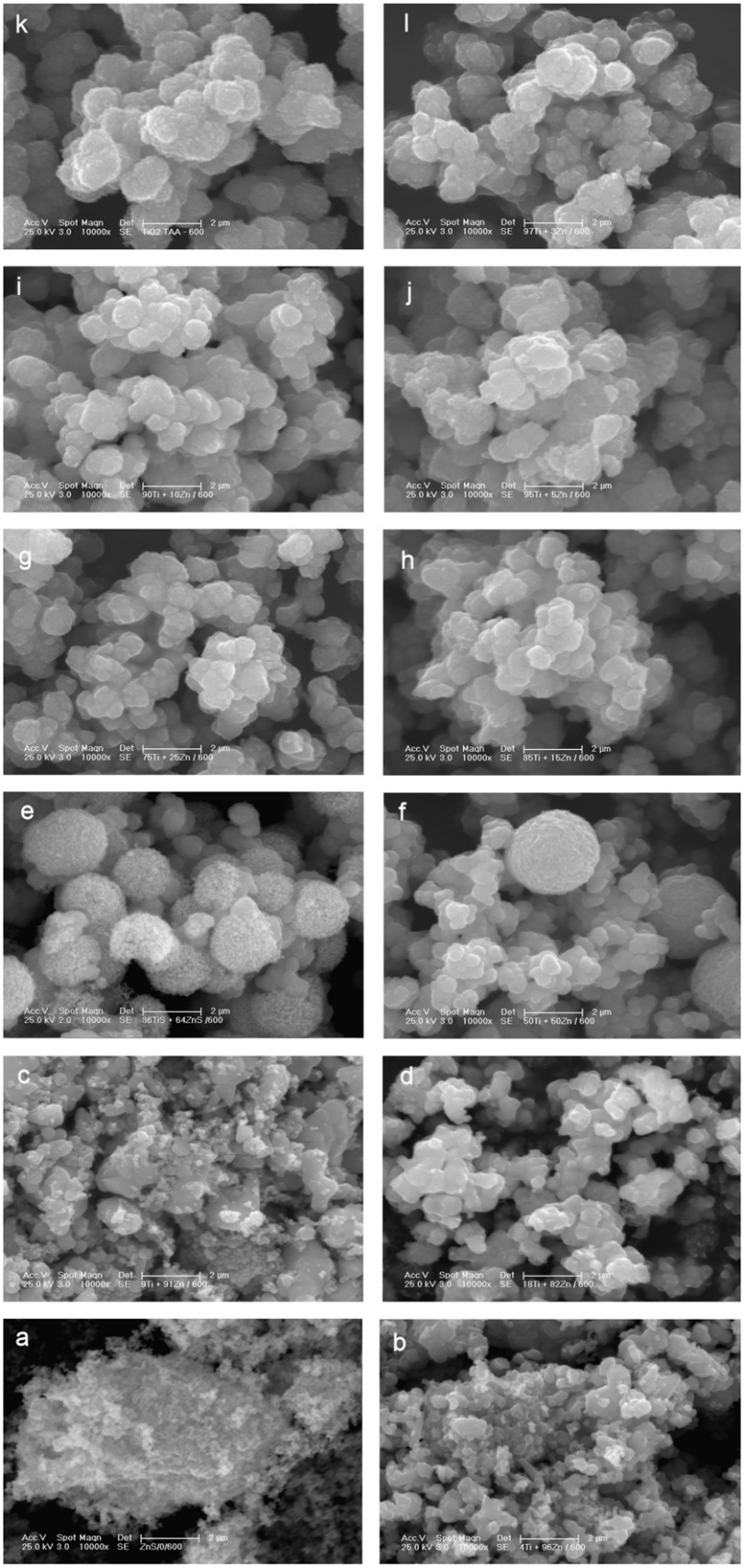

Fig. 3. SEM micrographs of particles prepared by homogenous hydrolysis and subsequent annealing at the temperature of 600 °C for 1 h in oxygen atmosphere. (a) TZO_0, (b) TZO_1, (c) TZO_2, (d) TZO_3, (e) TZO_4, (f) TZO_5, (g) TZO_6, (h) TZO_7, (i) TZO_8, (j) TZO_9, (l) TZO_10 and (k) TZO_11.

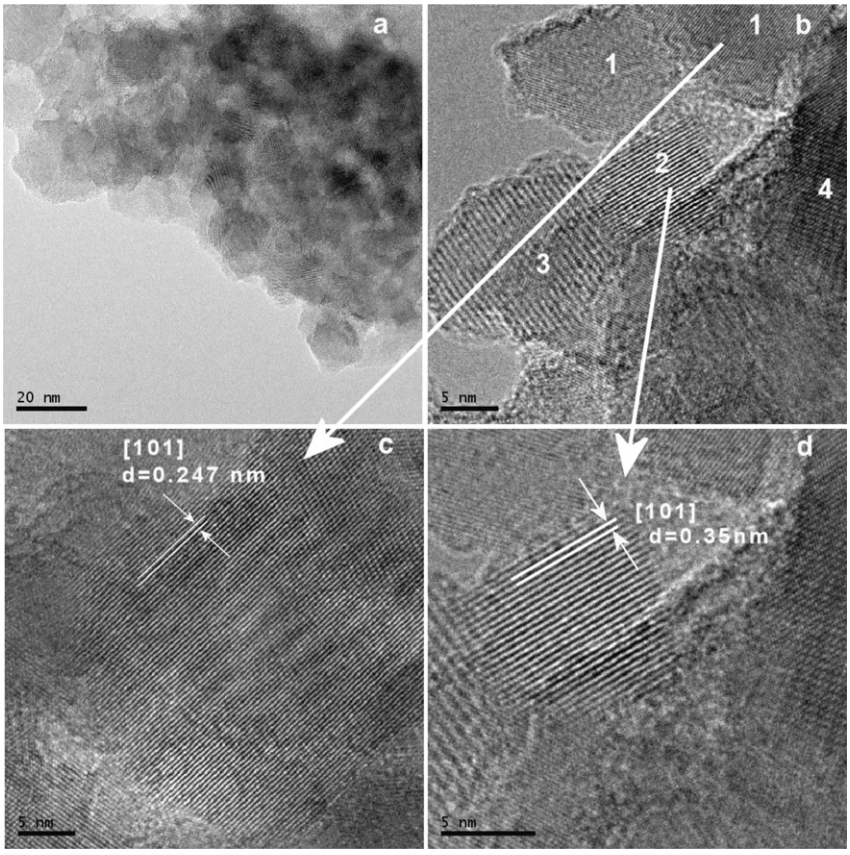

Fig. 4. (a) HRTEM micrographs of sample TZO_5; (b) 1—zincite phase, 2—anatase phase, 3—zinc titanium oxide phase, 4—rutile phase; (c) details of zincite phase; (d) details of anatase phase.

Table 3
Photodegradation rate of Orange II of prepared specimens and commercially available photocatalyst Degussa P25

Sample	Rate const. at 254 nm (min^{-1})	Rate const. at 365 nm (min^{-1})
TZO_0	0.0437	0.0211
TZO_1	0.0444	0.0355
TZO_2	0.0439	0.0194
TZO_3	0.0253	0.0114
TZO_4	0.0752	0.0209
TZO_5	0.0411	0.0086
TZO_6	0.0703	0.0092
TZO_7	0.1232	0.0155
TZO_8	0.0986	0.0121
TZO_9	0.0550	0.0120
TZO_10	0.0609	0.0233
TZO_11	0.0817	0.0340
P25 Degussa	0.0647	0.0471

and the optimum rate occurred with a lower catalyst loading than required at 350 nm. Hofstadler et al. [37] also showed that shorter wavelengths resulted in higher photocatalytic degradation process rates of 4-chlorophenol with small amounts of intermediates being formed. This is due to the fact that a shorter wavelength is associated with greater photon energy.

4. Conclusion

Nanocomposite of TiO_2/ZnO was prepared by homogeneous hydrolysis of zinc (II) sulphate and $TiOSO_4$ in aqueous solution at the temperature of 80 °C with TAA and subsequent annealing at the temperature of 600 °C. The solids consisted of uniform spherical aggregates in which the diameter of crystallites decreased with increasing amount of TiO_2.

It is obvious that BET surface areas (Table 1) are smaller in specimens doped with ZnO and annealed at higher temperatures. However, the photocatalytic activity of prepared samples was above average. Specimens doped with ZnO showed higher photodegradation rate of OII and the highest degradation rate was achieved on the sample denoted as TZO_7 ($k = 0.1232$) and all samples accomplished photocatalytic properties comparable to the standard Deggusa P25. Higher photocatalytic activity at 254 nm wavelength is given by higher band-gap energies of ZnO (3.3 eV) [38]. The higher photodegradation rate at 365 nm wavelength induces a smaller degradation rate at 254 nm wavelength.

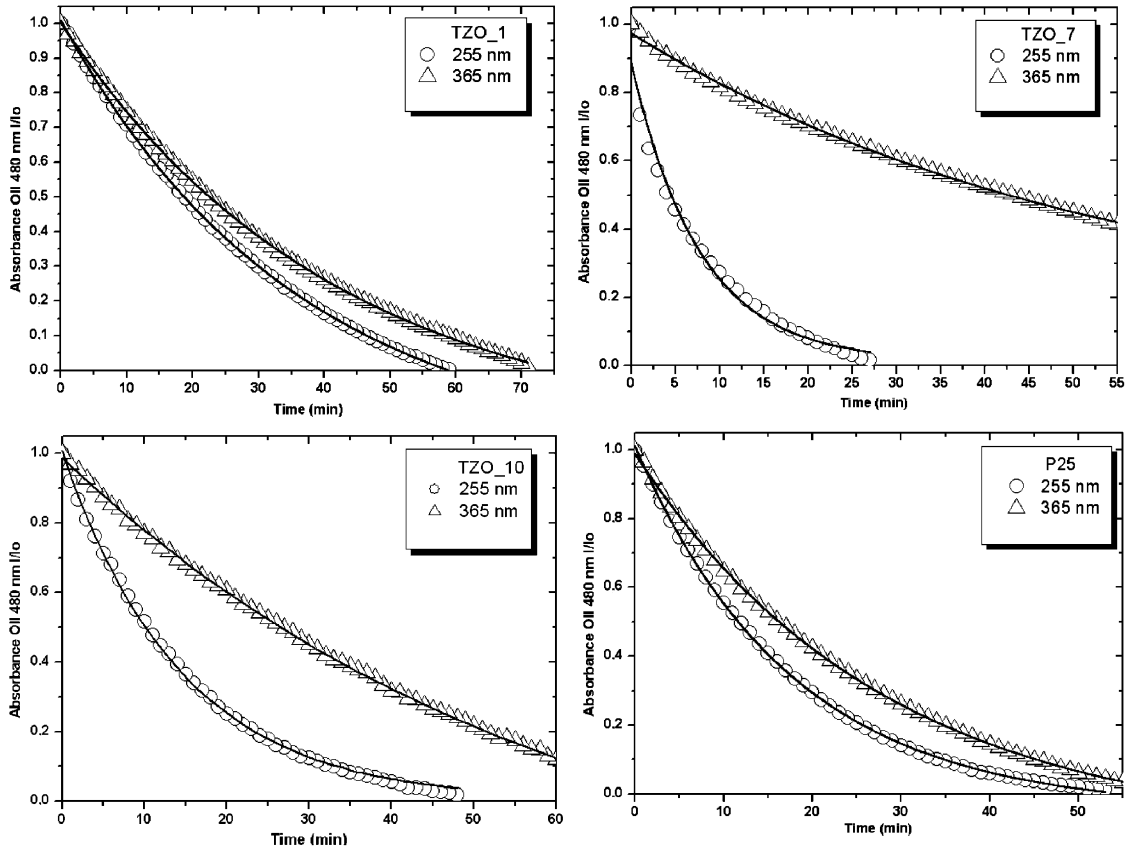

Fig. 5. Photodegradation of Orange II at wavelengths of 254 and 365 nm. Specimens of TiO_2/ZnO composite (TZO_1, TZO_7 and TZO_10) and the standard photocatalyst Degussa (P25).

Acknowledgement

This work was supported by the Academy of Sciences of the Czech Republic (Project no. AV OZ 40320502).

References

[1] A. Fujishima, T.N. Rao, D.A. Tryk, Titanium dioxide photocatalysis, J. Photochem. Photobiol. C: Photochem. Rev. 1 (2000) 1–21.
[2] A.A. Khodja, T. Sehili, J.F. Pilichowski, P. Boule, Photocatalytic degradation of 2-phenylphenol on TiO_2 and ZnO in aqueous suspensions, J. Photochem. Photobiol. A: Chem. 141 (2001) 231–239.
[3] C. Lizama, J. Freer, J. Baeza, H.D. Mansilla, Optimized photodegradation of reactive blue 19 on TiO_2 and ZnO suspensions, Catal. Today 76 (2002) 235–246.
[4] V. Houšková, V. Štengl, S. Bakardjieva, N. Murafa, A. Kalendová, F. Opluštil, Nanostructure materials for destruction of warfare agents and eco-toxins prepared by homogeneous hydrolysis with thioacetamide: part 1—zinc oxide, J. Phys. Chem. Solids 68 (2007) 716–720.
[5] J.-M. Herrmann, J. Disdier, P. Pichat, S. Malato, J. Blanco, TiO_2-based solar photocatalytic detoxification of water organic pollutants. Case studies of 2,4-dichlorophenooxyacetic acid (2,4-D) and of benzofuran, Appl. Catal. B: Environ. 17 (1998) 15–23.
[6] P.V. Kamat, Photochemistry on nonreactive and reactive (semiconductor) surfaces, Chem. Rev. 93 (1993) 267–300.
[7] M.R. Hoffmann, S.T. Martin, W. Choi, D.W. Bahnemann, Environmental applications of semiconductor photocatalysis, Chem. Rev. 95 (1995) 69–96.
[8] J. Bard, Design of semiconductor photoelectrochemical systems for solar energy conversion, J. Phys. Chem. 86 (1982) 172–177.
[9] M.A. Fox, M.T. Dulay, Heterogeneous photocatalysis, Chem. Rev. 93 (1993) 341–357.
[10] K. Kato, A. Tsuzuki, H. Taoda, Y. Torii, T. Kato, Y. Butsugan, Crystal structures of TiO_2 thin coatings prepared from the alkoxide solution via the dip-coating technique affecting the photocatalytic decomposition of aqueous acetic acid, J. Mater. Sci. 29 (1994) 5911–5915.
[11] R.R. Bacsa, J. Kiwi, Effect of rutile phase on the photocatalytic properties of nanocrystalline titania during the degradation of p-coumaric acid, Appl. Catal. B: Environ. 16 (1998) 19–29.
[12] V. Štengl, J. Šubrt, P. Bezdička, M. Maříková, S. Bakardjieva, Homogeneous precipitation with urea—an easy process for making spherical hydrous metal oxides, Solid State Phen. V 90–91 (2003) 121–126.
[13] H.-H. Ou, S.-L. Lo, Ch.-H. Wu, Exploring the interparticle electron transfer process in the photocatalytic oxidation of 4-chlorophenol, J. Hazardous Mater. B 137 (2006) 1362–1370.
[14] G. Marci, V. Augugliaro, M.J. López-Munoz, C. Martín, L. Palmisano, V. Rives, M. Schiavello, R.J.D. Tilley, A.M. Venezia, Preparation characterization and photocatalytic activity of polycrystalline ZnO/TiO_2 systems: 1. Surface and bulk characterization, J. Phys. Chem. B 105 (5) (2001) 1026–1032.
[15] S. Liao, H. Donggen, D. Yu, Y. Su, G. Juan, Preparation and characterization of ZnO/TiO_2, SO_4^{2-}/ZnO/TiO_2 photocatalyst and their photocatalysis, J. Photochem. Photobiol. A: Chem. 168 (2004) 7–13.
[16] M.S. El-Shall, D. Graiver, U. Pernisz, M.I. Baraton, Synthesis and characterization of nanoscale zinc oxide particles: I. Laser vaporization/condensation technique, NanoStruct. Mater. 6 (1995) 297–300.

[17] S. Hingorani, V. Pillai, P. Kumar, M.S. Multani, D.O. Shah, Microemulsion mediated synthesis of zinc-oxide nanoparticles for varistor studies, Mater. Res. Bull. 28 (1993) 1303–1310.
[18] D. Kaneko, H. Shouji, T. Kawai, K. Kon-No, Synthesis of ZnO particles by ammonia-catalyzed hydrolysis of zinc dibutoxide in nonionic reversed micelles, Langmuir 16 (2000) 4086–4089.
[19] T. Tani, L. Mädler, S.E. Pratsinis, Homogeneous ZnO nanoparticles by flame spray pyrolysis, J. Nanopart. Res. 4 (2002) 337–343.
[20] C.L. Carnes, K.J. Klabunde, Synthesis, isolation, and chemical reactivity studies of nanocrystalline zinc oxide, Langmuir 16 (2000) 3764–3772.
[21] M.F. Iskandar, K. Okuyama, F.G. Shi, Stable photoluminescence of zinc oxide quantum dots in silica nanoparticles matrix prepared by the combined sol–gel and spray drying method, J. Appl. Phys. 89 (2001) 6431–6434.
[22] M. Abdullah, S. Shibamoto, K. Okuyama, Synthesis of ZnO/SiO_2 nanocomposites emitting specific luminescence colors, Opt. Mater. 26 (2004) 95–100.
[23] M.A. Valenzuela, P. Bosch, J. Jiménez-Becerrill, O. Quiroz, A.I. Páez, Preparation, characterization and photocatalytic activity of ZnO, Fe_2O_3 and $ZnFe_2O_4$, J. Photochem. Photobiol. A: Chem. 148 (2002) 177–182.
[24] L. Jing, Z. Xu, X. Sun, J. Shang, W. Cai, The surface properties and photocatalytic activities of ZnO ultrafine particles, Appl. Surf. Sci. 180 (2001) 308–314.
[25] S.B. Park, Y.C. Kang, Photocatalytic activity of nanometer size ZnO particles prepared by spray pyrolysis, J. Aerosol Sci. 28 (1997) 473–474.
[26] X. Ren, D. Han, D. Chen, F. Tang, Large-scale synthesis of hexagonal cone-shaped ZnO nanoparticles with a simple route and their application to photocatalytic degradation, Mater. Res. Bull. 42 (2007) 807–813.
[27] J. Nishio, M. Tokumura, H.T. Znad, Y. Kawase, Photocatalytic decolorization of azo-dye with zinc oxide powder in an external UV light irradiation slurry photoreactor, J. Hazardous Mater. B 138 (2006) 106–115.
[28] S. Brunauer, P.H. Emmett, E. Teller, Adsorption of gases in multimolecular layers, J. Am. Chem. Soc. 60 (1938) 309–319.
[29] E.P. Barret, L.G. Joyner, P.P. Halenda, The determination of pore volume and area distributions in porous substances: I. Computations from nitrogen isotherms, J. Am. Chem. Soc. 73 (1951) 373–380.
[30] JCPDS PDF-2 release 2001, ICDD Newtown Square, PA, USA.
[31] A.L. Patterson, The Scherrer formula for X-ray particle size determination, Phys. Rev. 56 (1939) 978–982.
[32] V. Štengl, S. Bakardjieva, N. Murafa, V. Balek, V. Havlín, Optically transparent titanium dioxide particles incorporated in hydroxyethyl methacrylate thin layers, Adv. Synth. Catal., in press.
[33] J.M. Monteagudo, A. Durán, Fresnel lens to concentrate solar energy for the photocatalytic decoloration and mineralization of Orange 2 in aqueous solution, Chemosphere 65 (2006) 1242–1248.
[34] S. Lowell, J.E. Shields, Powder Surface Area and Porosity, Chapman & Hall, London, 1998.
[35] M. Macounová, H. Krýsová, J. Ludvík, J. Jirkovský, Kinetics of photocatalytic degradation of diuron in aqueous colloidal solutions of Q-TiO_2 particles, J. Photochem. Photobiol. A: Chem. 156 (2003) 273–282.
[36] R.W. Matthews, S.R. McEvoy, A comparison of 254 and 350 nm excitation of TiO_2 in simple photocatalytic reactors, J. Photochem. Photobiol. A: Chem. 66 (1992) 355–366.
[37] K. Hofstadler, R. Bauer, S. Novalic, G. Heisler, New reactor design for photocatalytic wastewater treatment with TiO_2 immobilized on fused silica glass fibers: photomineralization of 4-chlorophenol, Environ. Sci. Technol. 28 (1994) 670–674.
[38] A. Mang, K. Reimann, S. Rübenacke, Band gaps, crystal-field splitting, spin–orbit coupling, and exciton binding energies in ZnO under hydrostatic pressure, Solid State Commun. 94 (1995) 251–254.